



HAL
open science

Recent rheologic processes on dark polar dunes of Mars: Driven by interfacial water?

A. Null Kereszturi, D. Möhlmann, Sz. Berczi, T. Ganti, A. Kuti, A. Sik, A.
Horvath

► To cite this version:

A. Null Kereszturi, D. Möhlmann, Sz. Berczi, T. Ganti, A. Kuti, et al.. Recent rheologic processes on dark polar dunes of Mars: Driven by interfacial water?. *Icarus*, 2009, 201 (2), pp.492. 10.1016/j.icarus.2009.01.014 . hal-00533499

HAL Id: hal-00533499

<https://hal.science/hal-00533499>

Submitted on 7 Nov 2010

HAL is a multi-disciplinary open access archive for the deposit and dissemination of scientific research documents, whether they are published or not. The documents may come from teaching and research institutions in France or abroad, or from public or private research centers.

L'archive ouverte pluridisciplinaire **HAL**, est destinée au dépôt et à la diffusion de documents scientifiques de niveau recherche, publiés ou non, émanant des établissements d'enseignement et de recherche français ou étrangers, des laboratoires publics ou privés.

Accepted Manuscript

Recent rheologic processes on dark polar dunes of Mars: Driven by interfacial water?

A. Kereszturi, D. Möhlmann, Sz. Berczi, T. Ganti, A. Kuti, A. Sik, A. Horvath

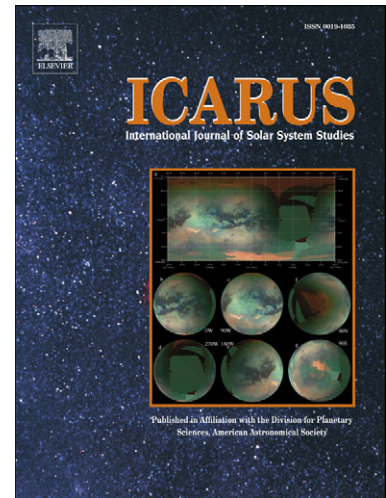
PII: S0019-1035(09)00035-9
DOI: [10.1016/j.icarus.2009.01.014](https://doi.org/10.1016/j.icarus.2009.01.014)
Reference: YICAR 8895

To appear in: *Icarus*

Received date: 16 September 2008
Revised date: 27 January 2009
Accepted date: 27 January 2009

Please cite this article as: A. Kereszturi, D. Möhlmann, Sz. Berczi, T. Ganti, A. Kuti, A. Sik, A. Horvath, Recent rheologic processes on dark polar dunes of Mars: Driven by interfacial water?, *Icarus* (2009), doi: [10.1016/j.icarus.2009.01.014](https://doi.org/10.1016/j.icarus.2009.01.014)

This is a PDF file of an unedited manuscript that has been accepted for publication. As a service to our customers we are providing this early version of the manuscript. The manuscript will undergo copyediting, typesetting, and review of the resulting proof before it is published in its final form. Please note that during the production process errors may be discovered which could affect the content, and all legal disclaimers that apply to the journal pertain.



1 Recent rheologic processes on dark polar dunes of Mars: Driven by interfacial water?

2

3 A. Kereszturi^{1,7,8}, D. Möhlmann², Sz. Berczi^{1,3}, T. Ganti¹, A. Kuti^{5,7}, A. Sik^{1,4}, A. Horvath^{1,6}

4

5 ¹ Collegium Budapest, Institute for Advanced Study, H-1041 Budapest, Szentharomsag 2.

6

Hungary

7

² DLR Institut für Planetenforschung, D-12489 Berlin, Rutherfordstr. 2. Germany,

8

³ Eotvos Lorand University of Sciences, Institute of Physics, H-1117 Budapest Pázmány 1/A.

9

Hungary

10

⁴ Eotvos Lorand University of Sciences, Institute of Geography and Earth Sciences, H-1117

11

Budapest Pázmány 1/c. Hungary

12

⁵ Eotvos Lorand University of Sciences, Institute of Physics, Department of Astronomy, H-

13

1117 Budapest Pázmány 1/c. Hungary

14

⁶ Konkoly Observatory, H-1525 Budapest Pf. 67. Hungary

15

⁷ Hungarian Astronomical Association, H-1461 Budapest, Pf. 219. Hungary

16

⁸ Károly Nagy Astronomical Foundation, H-1011 Budapest, Szekely u. 2-4., Hungary

17 Proposed running head: Seepages, rheology, infiltration, and erosion on Mars

18

19 Editorial correspondence to:

20 dr. Akos Kereszturi,

21 Collegium Budapest Institute for Advanced Study, H-1041 Budapest, Szentharomsag 2.

22 Hungary

23 E-mail address: akos@colbud.hu

24 **Abstract**

25

26 In springtime on HiRISE images of the Southern polar terrain of Mars flow-like or rheologic
27 features were observed. Their dark color is interpreted as partly defrosted surface where the
28 temperature is too high for CO₂ but low enough for H₂O ice to be present there. These
29 branching stripes grow in size and can move by an average velocity of up to about 1 m/day
30 and could terminate in pond-like accumulation features. The phenomenon may be the result of
31 interfacial water driven rheologic processes.

32

33 Liquid interfacial water can in the presence of water ice exist well below the melting point of
34 bulk water, by melting in course of interfacial attractive pressure by intermolecular forces
35 (van der Waals forces e.g.), curvature of water film surfaces, and e.g. by macroscopic weight,
36 acting upon ice. This melting phenomenon can be described in terms of “premelting of ice”. It
37 is a challenging consequence, that liquid interfacial water unavoidably must in form of
38 nanometric layers be present in water ice containing soil in the subsurface of Mars. It is the
39 aim of this paper to study possible rheologic consequences in relation to observations, which
40 seem to happen at sites of “dark dunes” on Mars at present.

41

42 The model in this work assumes that interfacial water accumulates at the bottom of a
43 translucent water-ice layer above a dark and insulated ground. This is warmed up towards the
44 melting point of water. The evolving layer of liquid interfacial water between the covering ice
45 sheet and the heated ground is assumed to drive downward directed flow-like features on
46 slopes, and it can, at least partially, infiltrate (seep) into a porous ground. There, in at least
47 temporarily cooler subsurface layers, the infiltrated liquid water refreezes and forms ice. The
48 related stress built-up is shown to be sufficient to cause destructive erosive processes. The
49 above-mentioned processes may cause change in the structure and thickness of the covering

50 ice and/or may cause the movement of dune grains. All these processes may explain the
51 observed springtime growing and downward extension of the slope streaks analyzed here.

52

53 Keywords: Mars, surface; ices; water, subsurface

ACCEPTED MANUSCRIPT

54

55 **1. Introduction**

56

57 Bulk water cannot stably exist at the thermodynamic conditions in a broad range of subzero-
58 temperatures present on Mars. However, liquid interfacial water must stably exist at these
59 temperatures also in the subsurface of Mars if the soil contains ice (Möhlmann 2004) and ice
60 must be present in the uppermost surface due to adsorption and freezing of atmospheric water
61 vapour, and/or the ice may also be a subsurface relict of earlier water rich Martian epochs.
62 Salts may influence the upper situation.

63

64 Liquid interfacial water in the H₂O-ice containing parts of the subsurface of Mars today may
65 be related to physical, chemical, and eventually also to biological processes (Möhlmann
66 2008). The presence of this interfacial water may be enhanced and extended to lower
67 temperatures in brines of various salts (Mellon and Phillips, 2001; Knauth and Burt 2002) and
68 may help destabilizing slope materials (Kossacki and Markiewitz 2008). Brass (1980)
69 analysed the freezing point of various salt-water systems on Mars and suggested freezing
70 point may be as low as 225 K. Interesting analogues have been discovered in the Antarctica
71 Dry Valleys with some liquid water related structures, resembling to Martian low latitude
72 slope streaks (Head et al. 2007a, Head et al. 2007b).

73

74 **2. Types of ices and frost in the analyzed terrains**

75

76 It is important to distinguish between the two kinds of ice covering the Martian surface:
77 carbon dioxide ice and water ice. The structure of these ice types (slab or porous) is not well
78 known, however it is possible to distinguish between the water and carbon dioxide ices on the
79 basis of their spectra, albedo and related surface temperature together. In this work, we

80 analyzed terrains by using satellite-born images, and TES albedo- and temperature values. In
81 every case we have indicated, which type of ice is probably on the surface, and which
82 parameters suggest the presence of that one, and the absence of the other kind of ice.

83

84 Hereafter first we present the observations and description of polar springtime surface
85 features, where springtime insolation gives rise to strange features resembling to those caused
86 by a flowing liquid. In the second part, a theoretical and modeling background to describe
87 these recent rheological phenomena is given, which is based on the at least temporary
88 presence of interfacial water in the uppermost surface layers. Detailed information about the
89 formation of this interfacial and adsorbed water layer on the soil grains can be found in the
90 references, here we only present some basic formulas in connection with the observed
91 structures.

92

93 The frost cover and its sublimation play an important role in the interpretation of our
94 observations. Both water and carbon dioxide ice can be present on the Martian surface inside
95 the seasonal caps. At the Northern Polar Region water ice forms a wide annulus at the
96 perimeter of the receding seasonal carbon dioxide ice cover (Kieffer and Titus 2001, Bibring
97 et al. 2005, Schmitt et al. 2005, Schmitt et al. 2006), partly because it appears from below the
98 sublimated carbon dioxide seasonal cap and partly because it recondenses onto the perimeter
99 of the remaining carbon dioxide ice (Wagstaff et al. 2008). Opposite to this situation at north,
100 no similar water ice annulus was observed at the Southern Polar Region, only smaller water
101 ice patches (Titus 2005, Langevin et al. 2006, Titus 2008) are present, which appear at the
102 perimeter of the receding annular carbon dioxide cap, and somewhere they are tens of
103 kilometers away from the bright permanent cap (Bibring et al. 2004) in summertime.

104

105 These observations can be interpreted, by assuming that a thin water ice layer below the
106 seasonal carbon dioxide frost is present, and water ice is left behind the sublimating carbon
107 dioxide ice cover. Such stratigraphy can be expected from theoretical reasons, too: when
108 seasonal cooling starts, ice condenses on the surface first from the cooling atmospheric water
109 vapor, and carbon dioxide (by its lower frost temperature) condenses later, forming a layered
110 structure. At the landing site of the Phoenix probe also water ice frost appeared first with the
111 cooling temperature in autumn (Lunar and Planetary Laboratory Press Release) as it was too
112 warm there to see any dry ice. This frost probably formed by direct condensation from the
113 atmosphere, although falling snowflakes were also observed by LIDAR on Phoenix (NASA
114 Press Release 2008).

115

116 The mentioned above observations and theoretical assumptions suggest that at polar terrains
117 on Mars, when the temperature is above the carbon dioxide frost point, and as long as the
118 surface is still frost covered, this frost is water ice.

119

120 **3. Appearance of the possible seepage features**

121

122 We observed dark slope structures emanating from Dark Dune Spots (DDSs) in the southern
123 terrain on MGS MOC (Horvath et al. 2001), and MRO HiRISE images. DDSs are a special
124 class of polar seasonal albedo features, their basic characteristics are the following: they are
125 round shaped low albedo structures on the seasonal frost-covered surface of dark dunes,
126 appear late winter, grow in size and number, and finally disappear with the disappearance of
127 seasonal frost in early summer. They are present in the Southern hemisphere between 65-80
128 degrees of latitude. (Although resembling seasonal dark albedo structures are present in the
129 northern hemisphere too, they are excluded this.)

130

131 The most important features related to DDSs are the elongated slope streaks (Horváth et al.
132 2001, Gánti et al. 2003, Szathmary et al. 2005). These slope structures always start from these
133 spots, at the analyzed terrain. These spots form special groups among the various ephemeral
134 seasonal albedo structures on Mars observed by different authors (Christensen et al. 2005;
135 Kieffer, 2003; Malin and Edgett, 2000; Piqueux et al. 2003).

136

137 DDSs generally show internal structures with a darker (umbra-like) central part, surrounded
138 by a lighter, outer (penumbra-like) ring – although there are many irregular shaped spots
139 among them. Their diameters vary between 5 and 200 m; and have a yearly reoccurrence to a
140 degree of 50-65%, meaning that about half of the spots appear very close (in meter scale
141 distance) to the location of spots from the previous year. Their most interesting aspect
142 analyzed in this work is the elongated structures on slopes, emanating from them.

143

144 Dark Dune Spots were analyzed previously on MGS MOC images (Horváth et al. 2001, Gánti
145 et al. 2003, Gánti et al. 2006, Kereszturi et al. 2007, Szathmary et al. 2007). Based on the
146 comparison of morphology, location and seasonal appearance of seasonal dark spots on new
147 HiRISE and earlier MOC images, we suggest the dark spots and slope structures observed in
148 the HiRISE images represent the same phenomena as earlier noted on MOC images (Fig. 1.).

149

150 The streaks emanating from these spots, form two groups. The larger group consists of
151 diffuse, fan shaped streaks, probably formed by the combination of CO₂ geyser activity and
152 winds (Kieffer et al. 2006) on slopes and horizontal terrains too. The second group has a
153 confined appearance (we call them confined streaks hereafter), which evolves during a later
154 seasonal phase. These are seen only on slopes (Kereszturi et al. 2007, 2008), when the surface
155 temperature is sufficiently high, and consequently less or no CO₂ ice cover is present.

156

157 The temperature values during this later seasonal phase are too high for the carbon dioxide ice
158 to cover the whole observed area. Unfortunately the spatial resolution of TES temperature
159 data is not high enough to observe precisely the area of these dark structures, so we cannot
160 determine are they free of CO₂ ice, but it is highly probable. If the temperature of a kilometer
161 sized terrain is higher than the CO₂ frost point, then CO₂ frost free areas can be expected to
162 exist. The mentioned above dark features must absorb more sunlight than their surroundings,
163 so they must be warmer than the average temperature of the observed area. Because of this
164 and the earlier observations of stratigraphic relationship of H₂O ice below CO₂ ice (see
165 section 2), it is possible that CO₂ ice is absent in the spots, and water ice left behind because
166 of the above mentioned layered structure.

167

168 On the analyzed HiRISE images both of the upper mentioned two slope streak groups, the
169 diffuse and the confined were also identified, as well on MOC images. On HiRISE images the
170 diffuse streaks turned out to consist of small (0,2-2 m) dark patches that form a discontinuous
171 fan-shaped structure. These small patches were visible as coalesced, continuous diffuse fans
172 in the lower resolution images of MGS MOC. The confined streaks, seen already on MGS
173 MOC images, look like continuous dark streaks on HiRISE images too.

174

175 **4. Method of slope streak analysis**

176

177 For the analysis we used HiRISE (MRO), HRSC (MEX), MOC (MGS) images, with
178 topographic data from MGS MOLA PEDR (Precision Experiment Data Record) dataset with
179 processing version L (Smith D. et al. 1999), and temperature data from TES (MGS)
180 measurements (Christensen 1992), using the “vanilla” software. Temperature data show
181 annual trend, and were derived for daytime around 2 pm, local true solar time. The surface
182 temperature values have spatial resolution of around 3 km, so they can be taken only as a

183 rough approach of the surface temperature of the whole analyzed dune complex. Another
184 source of uncertainty is that the temperature values were used only to realize a general annual
185 trend. These values can be taken as an orienting approach only to the conditions at the
186 observed locations and dates.

187

188 The change of seasonal albedo structures was analyzed on dunes inside three craters during
189 southern spring: Russel (54S 12E), an unnamed crater (68S 2E), and Richardson (72S 180E).
190 Only 11 of the analyzed HiRISE images of these craters showed confined slope streaks. Their
191 parameters can be seen in Table 1.

192

193 For temperature analysis we used MGS TES bolometer data, acquired in nadir-pointing mode
194 with “vanilla” software. Other data on Martian surface temperatures could be acquired from
195 THMEIS too, that has better spatial resolution but unfortunately observed rarely the same
196 terrain.

197

198 During the analysis we used the following terms to characterize the structures. The term
199 “slope streak” is used here only for those structures, which are analyzed in this paper,
200 although in the literature it is generally used for low latitude streaks formed possibly by the
201 mass wasting process of dust (Aharonson et al. 2003, Schorghofer et al. 2007, Beyer et al.
202 2008, Chuang et al. 2007). Here it is used for elongated structures that stretch in downward
203 direction on slopes, and emanate from DDSs. The term “movement” was used here for the
204 description of the change in the location of dark colored surface parts, and that probably, but
205 not necessarily means the real movement of any material. Theoretically changes in phase or
206 color at neighboring locations can also manifest in a similar phenomenon. We used the term
207 “flow front” for the advancing frontal section of these elongated dark slope structures, toward

208 the direction of their movement. Rheologic term is also used for the movement of material on
209 the surface or right below it.

210

211 **5. Morphology of slope structures**

212

213 The structures analyzed in this article were observed on dark dunes inside craters at the
214 southern hemisphere. These dunes are actually complexes of smaller dune units with size of
215 around 1 km, and the diameter of one complex is between 10 km and 20 km. The smallest
216 visible topographic structures are ripples on the top of the upper mentioned structures, with
217 width of 5 m - 20 m. During the observations the surface was covered with bright frost (at the
218 beginning CO₂, later possibly somewhere only H₂O), peppered with small Dark Dune Spots
219 and the slope features emanated from them. Analyzing nearly one hundred slope streaks on
220 HiRISE images, a characteristic sequence of events is visible that follows each other as the
221 season passes by. The phases of the DDS and related slope streak changes are:

222

- 223 1. A dark spot appears, at some occasions with fan shaped streaks emanating from it (it
224 can not be decided whether the spot appears first before the fan, or they appear at the
225 same time).
- 226 2. Confined streaks start emanate from DDSs in downward direction at slopes.
- 227 3. The branching pattern of the streaks becomes more developed and the streaks become
228 longer as time passes by. During this phase a brighter halo comes visible around both
229 the DDS and the slope streak, possibly related to some refreezing phenomenon.
- 230 4. With the advancement of seasons (towards summer) the dark parts become gray and
231 gradually reach the dark color of the whole dune complex.

232 5. The color/brightness of the whole terrain gets more and more homogeneous, and
233 finally only small signs of the previously observed dark albedo markings remain
234 visible.

235

236 In the second and third phases of the mentioned above sequence, slope streaks are obviously
237 present as dark features elongated downward on the slopes. For the determination of the
238 downward direction, we can use MOLA topography only in the cases of the largest slopes. In
239 most of the cases, the slope direction was identified on the basis of the lighting condition,
240 where the sunward slopes were generally brighter than the opposite ones (see Fig. 2. for
241 examples, where the Sun illuminates from the right, so the brighter slopes are tilted toward
242 the right). Slope streaks were observed only at those locations where the sloping angle was
243 high enough to produce obvious brightness differences between opposite slopes. Based on the
244 analysis of some individual MOLA measurements, the slope angle was somewhere between 5
245 and 20 degrees (here the horizontal plane has 0, the vertical 90 degree of slope angle).

246

247 The confined slope streaks always follow the sloping direction, regardless to the exposure of
248 the slope faces (e.g. north, south, east, west). No such preferred direction is visible among the
249 differently oriented slopes, although it is worth noting that homogeneous samples may hardly
250 exist because the dune crests in many cases are north-south oriented, probably by the general
251 east-west winds. This suggests that the slope angle value plays stronger role, than orientation
252 of the slope.

253

254 All the confined slope streaks visible in the mentioned above images emanate from the Dark
255 Dune Spots in downslope direction. They have characteristic appearance: forming a branching
256 network, where the smallest branch had a width of 3 - 6 m. This latter may be a characteristic
257 value, and it is equal to the average distance between the small dune ripples, which influence

258 their path like “channeling”. At many locations individual branches split into two branches
259 because of obstacle-forming ripples, and there are also cases where two or more branches
260 coalesce.

261

262 **6. Movement of slope streaks**

263

264 We use the term of movement for the downward stretch of the dark slope streaks emanate
265 from Dark Dune Spots as time passes by. Regarding the movement of the low albedo slope
266 streaks, we have observed the following:

267

- 268 • The dark slope streaks always start from the DDSs downward, regardless the fact, is
269 the DDS situated at the dune crest or on the slope itself – although more DDSs are
270 present at the top of a slope than on the slope. No streaks are visible without DDSs
271 (except for those cases where the DDS, that probably triggered the streak formation,
272 diminishes during the streak movement, possibly by some refreezing phenomenon).
273 This means that the processes, which trigger the formation of slope streaks are in
274 connection with DDSs. The reason for these processes may be related to the dark color
275 of the DDS that supports an increase of the temperature.
- 276 • All the confined streaks stretch downward on slopes, suggesting that gravity driven
277 effects dominate the development, opposite to the gas jet process, which forms fan
278 shaped streaks in various directions.
- 279 • The dark colored slope streaks become longer as time passes by in many cases – while
280 there were slope streaks, which did not grow during the same period, and did not show
281 any movement. In an earlier work (Horvath et al. 2008) we have shown that there is a
282 statistical connection between the length of a slope structure and the size of the

283 original DDS that may be valid here as well – although the situation seems to be more
284 complicated for slope streaks.

285 • The advancing flow front follows the several meter sized furrow-like depressions
286 between the small, probably wind-blown ripples.

287 • During the late phase of the dark material’s movement, sometimes the source region
288 became lighter, indicating possibly that the dark material has moved away, leaving
289 behind other stuff, or that the source region became covered by whitish frost again; or
290 if only phase changes have caused the dark color, the phase changed back again to the
291 original state of the source.

292 • The elongation of streaks takes place in the form of narrow, 2-10 m wide branches.
293 They are usually the darkest at their flow front, and get brighter upward with time.
294 During their advancement, in several cases the source region (the DDS itself) and the
295 upward part of the streak become brighter as time passes by. This observation may be
296 related to some kind of refreezing phenomena with a bright frost cover, or by the
297 cessation of any possible phase change that produced the originally dark color.

298 • On the bottom of the slopes, dark pond-like structures form where the streaks arrive at
299 a nearly horizontal surface, stop their movement, and probably accumulate and/or seep
300 into the near surface ground.

301

302 Based on the analysis of morphology and its changes in time, we have identified two
303 subgroups of confined streaks, emanating from dune spots: active and passive streaks (Fig.
304 3.). We use the term “active confined streak” for such streaks, which show evident signs of
305 gradual movement of dark fronts as the season passes by (Fig. 4.). In the case of “inactive
306 confined streaks”, no similar moving flow front was observable, and only the small and
307 separated dark parts became visible as the season passed by. With the progress of the spring
308 season, the dark areas grow, connect the separated parts and form a continuous streak. By the

309 end of this coalescence, the passive streak gains similar appearance to an active confined
310 streak. The elongated morphology suggests that these streaks have already moved in the past,
311 possibly during different climatic periods, but currently they only show a locally fixed
312 darkening without movement.

313

314 We have measured the movement speed of the flow fronts of active streaks for several
315 individual branches on subsequent images, where the same branch of certain slope streaks
316 could be firmly identified. The measured values were calculated for Martian days (sols) as an
317 average value, as if the whole movement had happened during a full Martian sol. If the theory
318 described in this paper can be applied, a thin liquid film of interfacial water lubricates the
319 grains. The resulting movement may take place only during a small part of a Martian day,
320 probably when the temperature and water content produce a sufficiently thick layer of
321 undercooled liquid interfacial water. Also freezing may cause expansion and failure inside the
322 dunes' structure (see in section 8.3).

323

324 The observed average motion speed of flow fronts has been estimated to be of up to 1.4 m/sol.
325 There were many occasions where the dark stuff did not move, or moved slower than 0.1
326 m/sol. Where the movement was obvious, it usually happened on meter scale distance on the
327 average on a Martian day (Fig. 5.). This suggests the presence of some critical limit above
328 which the movement took place, and that it happens at a reasonable distance.

329

330 **7. Connection between temperature and morphology**

331

332 We have analyzed average annual TES based surface temperatures and the related
333 morphology of the slope streaks. The three observed craters were situated at different latitude,
334 at 54S, 68S and 72S. As a result, during the springtime warming the average surface

335 temperature reaches certain values later in solar longitude for locations farther from the
336 equator. If the beginning of the dark streaks' movement takes place after the temperature has
337 reached a critical value, it is expected that the movement starts later closer to the south pole.

338

339 We have studied the annual temperatures (Fig. 6., 7., 8.), with continuous TES based datasets,
340 but regarding the images unfortunately there is no continuous coverage of the whole spring
341 period available. The first indications of streak movement can be observed earlier in
342 Richardson crater than in Russel crater, because for Russel no image is available for the
343 critical period. So, it was not yet possible to establish a direct relation between the first
344 appearance of streaks and the seasonal increase in temperatures.

345

346 The TES temperature values can be taken only as a rough approach for the surface
347 temperatures. Because of the comparatively low spatial resolution of the detector, it cannot
348 resolve certain parts of the dark features, which may be warmer than the measured "average"
349 value. In spite of this restriction, the streaks' movement started around the same temperature
350 in Russel, the unnamed crater, and probably in Richardson crater too, but there the situation is
351 somewhat different, as described below in more in detail.

352

353 Analyzing the average annual temperature trend and the changes in streaks' morphology, the
354 streaks appeared in Russel and the unnamed crater when the temperature was between 180 K
355 and 200 K. In Richardson crater the situation is different: the first indication of the slope
356 streak movement there appeared on the images acquired at $L_s=210.6$, when the average
357 temperature is not much above the frost point of carbon dioxide. But the temperature curve
358 has already started to rise, suggesting that there must be warmer locations free of CO_2 frost on
359 the surface, but they are probably below the limit of the spatial resolution. These warmer

360 small patches may be the dark features, because their much lower albedo causes a warm-up in
361 course of the increasing insolation.

362

363 In general, and based on TES temperature data, it can be stated that during the movement of
364 slope structures, a large part of the surface (or the whole observed area) is free of carbon
365 dioxide ice, as the temperature of the dark slopes is above the CO₂ freezing point. At the same
366 time, based on the images, frost covers most of the terrains, so that frost is probably
367 composed of water ice. As a conclusion the dark slope streaks are active during a seasonal
368 phase when water ice is probably present and exposed to the surface in the analyzed regions.

369

370 Because of the small number of available HiRISE images of the slope movement phenomena
371 and the lack of continuous data sets, the exact determination of the appearance /
372 disappearance of slope structures is not yet possible. But several important conclusions can
373 already be drawn from the available images. Based on the comparison of images and
374 temperature data from different latitudes, the flow-like (or rheologic) process seems to start
375 when the temperature is above the carbon dioxide frost point, around about 180 - 200 K. The
376 movements usually take place on a meter scale distance per day. The phenomenon of an
377 undercooled liquid interfacial water layer may help to understand these movements on slopes,
378 as described below.

379

380 **8. Liquid interfacial water on Mars**

381

382 Around hydrophilic mineral grains embedded in snow/ice, a layer of liquid interfacial water
383 must form between the mineral surface and the snow/ice (Möhlmann, 2008). The reason is the
384 freezing point depression due to the attractive pressure between the surfaces of water-
385 snow/ice and the mineral. This can also for surfaces of ice (without a mineral counterpart) be

386 described in terms of "premelting" of ice (Dash et al., 2006) by attractive van der Waals force
 387 acting upon the uppermost surface layers of snow/ice (cf. Fig. 9).

388 This attractive van der Waals force F_{vdW} , acting per area F upon the surface of ice of volume
 389 $V = F d$ on a mineral surface F is given in case of parallel interfaces by

$$390 \quad F_{vdW} = \frac{A_{lm}}{6\pi d^3} F. \quad (1)$$

391 A_{lm} is the Hamaker constant for the interaction of substances "l" (ice) and "m" (mineral) in
 392 presence of interfacial water "l" in between. This force acts also between the molecules of
 393 water ice at and very near to the surface of ice, which therefore is prone to "premelting". This
 394 configuration is described schematically in Fig. 10. The related depressed freezing
 395 temperature can in general be shown to be related to different acting pressures, as interfacial
 396 melting (premelting) via F_{vdW} , via curvature melting in course of surface tension, and pressure
 397 melting via $(p_L - p_m)(\rho_S/\rho_L) - 1$ by

$$398 \quad \rho_S q \frac{T_m - T}{T_m} = \frac{A}{6\pi d^3} + \kappa\sigma + (p_L - p_m) \left(\frac{\rho_S}{\rho_L} - 1 \right). \quad (2)$$

399 (cf. Dash et al., 2006, Wettlaufer and Worster, 2006). T_m is the standard melting temperature,
 400 $\Delta T = T_m - T$ is called the freezing point depression, q is the latent heat, ρ and p represent
 401 mass density and pressure, respectively, and the indices L and S indicate the solid (i.e. ice)
 402 and the liquid state.

403

404 The limiting minimum temperature of the liquid phase of the water layer below the bulk
 405 melting temperature T_m is in case of acting van der Waals forces only, given by

$$406 \quad T = T_m \left(1 - \frac{A}{6\pi q \rho_S d^3} \right). \quad (3)$$

407 Fig. 11. shows the limiting minimum temperature for interfacial water to remain liquid in
 408 dependence on layer thickness and for the range of typical Hamaker constants in nature. As
 409 shown in Fig. 12., interfacial water may exist down to about 150 K, as it has experimentally

410 been verified by Person and Derbyshire (1974). Furthermore, the existence of “unfrozen”
411 water in subzero temperature soils has also been demonstrated and studied by Anderson
412 (1968) and Anderson et al. (1973). Note that the thickness of the layer of undercooled liquid
413 interfacial water is often measured in film-like “monolayers” (of 0.35 nm), which are to be
414 understood as an orienting average value, not as a stringent geometrical model.

415

$$416 \quad d = \left(\frac{A T_m / 6\pi}{\rho_s q \Delta T} \right)^{1/3} \quad (4)$$

417

418 This limiting temperature can get lowered in brines by adding salts, which also tend to
419 increase the thickness d of the layer. Fig. 11. and 12. indicate that liquid interfacial water must
420 exist on Mars in a temperature band below the melting temperature. These temperatures can
421 be reached at polar latitudes at daytime conditions and in the vicinity of the snow/ice interface
422 above an insolation-heated ground, and it can remain “stable” for hours until the ice has left
423 by daytime sublimation or until cooling starts at late afternoon hours (cf. Fig. 12.).

424

425 Comparatively high sub-surface temperatures, which may approach the melting point (with
426 the consequence of possible temporary melting) can be expected in course of effective cooling
427 at the surface of insulated ice/snow (due to sublimation and RI re-radiation) but with heat
428 accumulation in an insolation-absorbing sub-surface, if the thermal conductivity is sufficient
429 small. At least, this will strengthen the possible appearance and amount of interfacial water.

430

431 Undercooled liquid interfacial water will be able to flow downhill on slopes, being that way a
432 driver of rheologic processes, and parts of it also may seep downward into the subsurface.
433 This infiltrated water will refreeze in the cooler lower subsurface layers. Resulting erosion
434 can modify these layers, since ice is of an about 9% larger volume than the liquid interfacial

435 water. The final result will finally be a stress built-up in the upper subsurface. This may lead
 436 to cracks, failures and erosive processes (cf. Fisher 2005).

437

438 **8.1 Liquid interfacial water in soil**

439

440 The content of liquid interfacial water in porous soil of specific surface S_M , dry mass m_{dry} and
 441 mass $M_{\text{H}_2\text{O}}$ of liquid interfacial water can simply be estimated via

$$442 \quad a_m(T,d) = \frac{M_{\text{H}_2\text{O}}(T,d)}{m_{\text{dry}}} = \rho_{\text{H}_2\text{O}} S_M d = S_M \rho_{\text{H}_2\text{O}} \left(\frac{A T_m}{6\pi\eta\rho_s \Delta T} \right)^{1/3}. \quad (5)$$

443

444 Fig. 13 shows measured and modeled (by eq. (5)) soil water contents for four different
 445 montmorillonites. Obviously, the content of “microscopic”, better “nanometric”, liquid
 446 interfacial water in frozen soil is a macroscopically relevant phenomenon. It may well reach
 447 several 10%. This phenomenon is well known as “unfrozen” water in terrestrial permafrost.
 448 Analogously to terrestrial permafrost, undercooled liquid interfacial water can on Mars
 449 preferably in springtime and after removal of the CO_2 -ice cover evolve at sites of the water-
 450 ice covered parts of the polar caps in course of their warming.

451

452 **8.2 Rheologic phenomena (downslope flows)**

453

454 The insulated but yet frozen and dark ground on slopes may become the cause of a
 455 gravitationally driven flow-like down-slope transport of the interfacial water, preferably
 456 between the translucent covering water ice layer and the warmer ground, which is heated by
 457 insolation (cf. Fig. 14.) towards the melting point temperature. The resulting layer of
 458 interfacial water will be able to remain at or near to the melting temperature over longer time-
 459 spans of hours or so, and thus it must form several monolayers of undercooled liquid

460 interfacial water (cf. Fig. 11.). Thus, there can on inclined surfaces, as slopes, form rheologic
 461 features as down-flow phenomena. Fig. 14 illustrates that situation. The thickness of that layer
 462 is the greatest at temperatures in the vicinity of the melting temperature (cf. Fig. 11.).
 463 Depending on grain sizes, that can in the 10 nm range (and less) become sufficient also for
 464 capillary effects to get involved in this wetting and transport process.

465

466 The flow of liquid interfacial water will be counteracted by friction within the liquid layer.
 467 The resulting stationary velocity v of a particle of radius R within the liquid layer is given
 468 then by

$$469 \quad v = \frac{2R^2 (\rho_p - \rho_w) g \sin \alpha}{9 \eta}, \quad (6)$$

470 The viscosity η is given by $\eta = 1.38 \cdot 10^{-3}$ Pa s (Rempel et al., 2001), g is the gravitational
 471 acceleration on the surface, α is the inclination of the slope, and ρ_p and ρ_w are the mass
 472 densities of the particle and of the water, respectively. Obviously, diurnal downslope flow
 473 distances up to about 1 m can be estimated to be reachable in case of the above described
 474 slope model (Fig. 15.).

475

476 Fig. 5., 6., 7., 8. give examples of possibly related flow-like features on a Martian slope, as
 477 observed by HiRISE and studied in the view of the propagation properties by A. Kereszturi et
 478 al. at Collegium Budapest (Kereszturi et al. 2008). The diurnal progress is about 1 m, but
 479 these flow-like movements can, of course, be effective over only a few hours a day. So, the
 480 real propagation velocity in the few daily “active hours” is correspondingly larger. Probably,
 481 the presence liquid interfacial water can also have an influence on its optical properties by
 482 solving coloring chemical substances from the solid subsurface materials, what can support
 483 the heating process further.

484

485 8.3 Erosion and failure

486

487 In water-filled pores, refreezing of liquid undercooled interfacial water ice will cause erosion.

488 The phase change from liquid water to ice results in volume increase (ΔV) of about $\Delta V/V =$

489 9% and will cause a pressure or elastic stress in the ice/mineral matrix. This stress can cause

490 failure and cracks with erosive results. Therefore, erosion advances in course of refreezing of

491 interfacial water, when the seasonal temperatures approach the local freezing point

492 temperature. In case of the presence of a water ice cover of the surface, seepage and

493 infiltration of interfacial water and its refreezing in the subsurface will happen when the frost

494 point temperature will be reached daytime (in spring) and will decrease below during

495 nighttime.

496

497 The erosive stress τ due to refreezing water can be estimated via

$$498 \quad \tau = \frac{E}{1-2\nu} \frac{\Delta V}{V}. \quad (8)$$

499 E is Young's modulus, and ν is Poisson's constant. Typical values for snow and water ice are

500 $E \approx (1-10) 10^9$ Pa, and $\nu \approx 0.2 - 0.5$ given by Mellor (1975). With $\Delta V/V = 0.09$, this

501 indicates that the related stress can cause erosive destruction around 1 GPa. For materials to

502 fail by brittle structure, there is usually a linear correlation between uniaxial compressive

503 strength σ and Young's modulus with $\sigma/E \approx (2 - 3) 10^{-3}$ (Mellor, 1975). Compressive

504 stresses are for snow between (1 - 10) MPa (Mellor, 1975). Therefore, refreezing driven

505 stresses can become the cause of erosive destruction in ice/snow mixtures.

506

507 9. Conclusions

508

509 Based on observations, narrow, confined, dark slope streaks emanate from Dark Dune Spots
510 during local spring at the observed three craters. These streaks always start from features
511 called Dark Dune Spots, they stretch and move downward, and follow the topography of the
512 depressions between the small scale ripples, producing a branching pattern. Gravity-driven
513 processes can let streaks grow in time, with a speed up to 1.4 meter/sol, as derived from
514 observations. This agrees in the order of magnitude with model estimates. These movements
515 were observed when the temperature was above the carbon dioxide frost point, and up to ~
516 250 K, suggesting that this process is not related to carbon dioxide frost and therefore is
517 possibly connected to liquid interfacial water, if water ice is inside the spots. After the
518 darkening of a certain surface area, brightening may follow as the dark flow front has passed
519 by, probably by refreezing of frost, or the phase change of surface material. Unfortunately
520 today only CRISM data has enough spatial resolution to analyze the possible presence of
521 water ice inside spots, but the publicly available data does not meet the required locations and
522 seasonal periods together.

523

524 Taking the assumption that water ice is present inside the spots, interfacial water driven
525 process may produce the observed phenomena. Based on thermodynamics, it can be stated,
526 that interfacial liquid water must, at least temporarily, be present on the Martian surface,
527 particularly in the shrinking and warming seasonal water ice covered terrain. Rheologic, flow-
528 like phenomenon at inclined surfaces, which are caused by liquid interfacial water between a
529 covering ice sheet and the warmed-up mineral surface are therefore to be expected to happen
530 on present Mars. As a result, interfacial water may produce change in the appearance of the
531 dune' surface by 1. seeping and causing sublimation of surface frost cover, 2. by produce
532 sliding of lubricated grains above each other and 3. by refreezing produced stress and
533 movement in the grain structure. Our computations and model show that such processes are
534 reasonable under the present surface conditions and satisfactorily interpret the observed

535 movement of springtime streaks. The presence of interfacial water at the observed features
536 even may have astrobiological consequences (Horváth et al. 2001, Gánti et al. 2003, Pocs et
537 al. 2004, Szathmary et al. 2007) too.

538

539 **14. Acknowledgment**

540

541 This work was supported by the ESA ECS-project No. 98076 and the Pro Renovanda Cultura
542 Hungariae Foundation, Student Science Fellowship Award.

543 **15. References**

544

545 Aharonson, O., Schorghofer N., Gerstell, F.M., 2003. Slope streak formation and dust
546 deposition rates on Mars. *J. of Geophys. Res.* 108, E12, 5138, doi:10.1029/2003JE002123.

547

548 Anderson, D.M., 1968. Undercooling, Freezing Point Depression, and Ice Nucleation of Soil
549 Water, *Israel Journal of Chemistry*, 6, 349-355.

550

551 Anderson, D.M., Tice A.T., McKim, H.L. 1973. The unfrozen water and apparent specific
552 heat capacity of frozen soils, in *North American Contribution, Permafrost*, second. Internatl.
553 Conference, 289-296, Yakutsk, National Academy of Sciences, Washington D.C.

554

555 Beyer, R.A.; Chuang, F.C., Thomson, B.J., Milazzo, M.P., Wray, M. P., 2008. Martian Slope
556 Streak Brightening Mechanisms, 39th Lunar Planet. Sci. Conf. abstract 2538.

557

558 Bibring, J. P., Langevin, Y., Poulet, F., Gendrin A., Gondet, B., Berthé, M., Soufflot, A.,
559 Drossart, P., Combes, M. Bellucci, G., Moroz, V., Mangold, N., Schmitt, B. & the OMEGA
560 team, 2004. Perennial water ice identified in the south polar cap of Mars, *Nature*, 428, 627-
561 630.

562

563 Bibring, J.P., Y. Langevin, A. Gendrin, B. Gondet, F. Poulet, M. Berthe, A. Soufflot, R.
564 Arvidson, N. Mangold, J. Mustard, P. Drossart & the OMEGA team, 2005. Surface diversity
565 as revealed by the OMEGA/Mars Express Observations, *Science*, 307, 1576–1581

566

567 Bodnar, R.J., 2001. PTX phase equilibria in the H₂O-CO₂-salt system at Mars near-surface
568 conditions. 32th Lunar Planet. Sci. Conf., abstract 1689.

569

570 Brass, G.W., 1980. Stability of brines on Mars, *Icarus*, 42, 20–28.

571

572 Christensen, P., Anderson, D., Chase, S.C., Clark, R.N., Kieffer, H.H., Malin, M.C., Pearl,
573 J.C., Carpenter, J.B., Nuno, B.F., 1992. Thermal Emission Spectrometer Experiment: Mars
574 Observer Mission, *J. of Geophys. Res.*, 97, 7719-7734.

575

576 Christensen, P.R.; Kieffer, H.H., Titus, T.N., 2005. Infrared and Visible Observations of
577 South Polar Spots and Fans, American Geophysical Union, Fall Meeting, abstract P23C-04.

578

579 Chuang, F.C.; Beyer, R.A., McEwen, A.S., Thomson, B.J. 2007. HiRISE observations of
580 slope streaks on Mars, *Geophysical Research Letters*, 34/20, CiteID L20204.

581

582 Clow, G.D., 1987. Generation of liquid water on Mars through the melting of a dusty
583 snowpack, *Icarus* 72, 95-127.

584

585 Dash, J.G., Rempel, A.W., Wettlaufer, J.S., 2006. The physics of premelted ice at its
586 geophysical consequences, *Annu. Rev. Fluid Mech.*, 38, 427-452.

587

588 Fisher D.A., 2005. A process to make massive ice in the Martian regolith using long-term
589 diffusion and thermal cracking, *Icarus*, 179, 387–397.

590

591 Gánti, T., Horváth, A., Bérczi, Sz., Gesztesi, A., Szathmáry, E. 2003. Dark dune Spots:
592 Possible Biomarkers on Mars? *Origins of Life and Evolution of the Biosphere*, 33, 515-557.

593

594

- 595 Gánti T., Bérczi, Sz., Horváth, A., Kereszturi, A., Pócs, T., Sik, A., Szathmáry, E., 2006.
596 Hypothetical time sequence of the morphological changes in global and local levels of the
597 dark dune spots in polar regions of Mars, 37th Lunar Planet. Sci. Conf., abstract 1918
598
- 599 Haberle, R.M., McKay, C.P., Schaeffer, J., Cabro, N.A., Grin, E.A., Zent A.P. and Quinn, R.,
600 2001. On the possibility of liquid water on present-day Mars. *J. Geophys. Res.* 106, E10,
601 23317–23326.
602
- 603 Hamaker, H.C., 1937. The London-van der Waals Attraction between Spherical Particles,
604 *Physica*, IV, 10, 1058.
605
- 606 Head, J.W., Marchant, D.R., Dickson, J.L., Levy, J.S. and Morgan, G.A., 2007a. Slope
607 streaks in the Antarctic Dry Valleys: characteristics, candidate formation mechanisms, and
608 implications for slope streak formation in the Martian environment, 7th International Conf. on
609 Mars, abstract 3114.
610
- 611 Head, J.W., Marchant, D.R., Dickson, J.L., Levy, J.S., Morgan, G.A., Kreslavsky M., 2007b.
612 Mars gully analogs in the Antarctic Dry Valleys: geological settings and processes, 7th
613 International Conf. on Mars, abstract 3118.
614
- 615 Hecht, M.H., 2002. Metastability of Liquid Water on Mars, *Icarus*, 156, 373–386,
616 doi:10.1006/icar.2001.6794.
617
- 618 Horváth, A., Gánti T., Gesztes A., Bérczi Sz., Szathmáry E. 2001. Probable evidences of
619 recent biological activity on Mars: appearance and growing of dark dune spots in the south
620 polar region, 32nd Lunar Planet. Sci. Conf., abstract 1543.

621

622 Horváth, A. Kereszturi, Á. Bérczi, Sz. Sik, A., Pócs, T., Gesztesi, A., Gánti, T., Szathmáry, E.
623 2005. Annual change of Martian DDS-seepages, 35th Lunar and Planet. Sci. Conf., abstract
624 1128.

625

626 Horváth, A., Kereszturi, Á., Bérczi, Sz., Sik, A., Pócs, T., Ganti, T. & Szathmáry, E. 2009.
627 Analysis of dark albedo features on a Southern Polar dune field of Mars, Astrobiology in
628 press

629

630 Kereszturi, A. Sik, Horvath, A., D. Reiss, Jaumann, R., Neukum G., 2007. Season-dependent
631 behavior of Dark Dune Spots on Mars, 38th Lunar and Planet. Sci. Conf., abstract 1864.

632

633 Kereszturi, A., Möhlmann, D., Berczi, Sz., Horvath, A., Ganti, T., Kuti, A., Pocs, T., Sik, A.,
634 Szathmary, E., 2008. Analysis of possible interfacial water driven seepages on Mars, 39th
635 Lunar and Planet. Sci. Conf., abstract 1555.

636

637 Kieffer, H.H., Titus, T.N., 2001. TES Mapping of Mars' North Seasonal Cap, Icarus, 154,
638 162-180.

639

640 Kieffer, H.H., 2003. Behavior of Solid CO₂ on Mars: A Real Zoo. 6th International Conf. on
641 Mars, abstract 3158.

642

643 Kieffer, H.H., Christensen, P.R., Titus, T.N., 2006. CO₂ jets formed by sublimation beneath
644 translucent slab ice in Mars' seasonal south polar ice cap, Nature, 442, 793-796.

645

- 646 Knauth, L.P., Burt, D.M., 2002. Eutectic Brines on Mars: Origin and Possible Relation to
647 Young Seepage Features, *Icarus*, 158, 267–271.
648
- 649 Kossacki, K.J., Markiewicz, W.J., 2008. Martian hill-gullies, surface and sub-surface
650 moisture, Mars Water Cycle Workshop, Paris.
651
- 652 Langevin, Y., Bibring, J.P., Douté, S., Vincendon, M., Poulet, F., Gondet, B., Schmitt, B.,
653 Forget, F., Montmessin, F. and the OMEGA team. 2006. CO₂ ice and H₂O ice in the seasonal
654 caps of Mars during the spring retreat, phase. 4th Mars Polar Sci. Conf., abstract 8091.
655
- 656 Malin, M.C., Edgett, K.S., 2000. Frosting and defrosting of Martian polar dunes, 31th Lunar
657 and Planet. Sci., abstract 1056.
658
- 659 Mellon, M., 1975. A review of basic snow mechanics. Snow Mechanics symposium 251,
660 IAHS Publ. 114.
661
- 662 Mellon, M.T., Phillips, R.J., 2001. Recent gullies on Mars and the source of liquid water, *J.*
663 *Geophys. Res.*, 106, 0, 1–15.
664
- 665 Motazedian, T., 2003 Currently Flowing Water on Mars. 34th Lunar Planet. Sci. Conf.,
666 abstract 1840.
667
- 668 Möhlmann, D., 2004. Water in the upper Martian surface at mid- and low-latitudes: presence,
669 state, and consequences, *Icarus*, 168, 318-323.
670

- 671 Möhlmann, D., 2008. The influence of van der Waals forces on the state of water in the
672 shallow subsurface of Mars, *Icarus*, 195, 131-139.
673
- 674 NASA Press Release 2008. no. 08-246, 2008.09.29.
675
- 676 Pearson, T.T., Derbyshire, W., 1974. NMR studies of water adsorbed on a number of silica
677 surfaces, *J. Coll. Interf. Sci.*, 46 (2), 232–248.
678
- 679 Piqueux, S., Byrbe, S. Richardson, M.I., 2003. Sublimation of Mars's Southern seasonal CO₂
680 ice cap and the formation of spiders. *J. Geophys. Res.*, 108, 5084.
681
- 682 Pócs, T., Horváth, A., Gánti, T., Bérczi, Sz., Szathmáry, E., 2004. Possible Crypto-Biotic-
683 Crust on Mars? In: *Exo/Astrobiology, Proc. Third Eur. Workshop, ESA SP-545*, 265-266.
684
- 685 Reiss, D., van Gasselt, S., Neukum, G., Jaumann, R., 2004. Absolute dune ages and
686 implications for the time of formation of gullies in Nirgal Vallis, Mars. 35th Lunar Planet.
687 Sci. Conf., abstract 1639.
688
- 689 Rempel, A.W., Wettlaufer, J.S., Worster, M.G., 2001. Interfacial premelting and the
690 thermomolecular Force: Thermodynamic Buoyancy, *Phys. Rev. Lett.*, 87 No.8, 088501-504.
691
- 692 Ryan, J.A., Sherman, R.D., 1981. H₂O Frost Point Detection on Mars?, *J. Geophys. Res.*, 86,
693 C1, 503-511.
694

695 Schmitt, B., Douté, S., Langevin, Y., Forget, F., Bibring, J.P., Gondet, B. & the OMEGA
696 Team. 2005. Northern Seasonal Condensates on Mars by Omega/Mars Express, 6th Lunar
697 Planet. Sci. Conf., abstract 2326.

698

699 Schmitt, B., Schmidt, F., Douté, S., Langevin, Y., Forget, F., Bibring, J.P., Gondet, B. and the
700 OMEGA Team, 2006. Recession of the northern seasonal condensates on mars by
701 OMEGA/Mars Express, 4th Mars Polar Sci. Conf., abstract 8050.

702

703 Schorghofer, N.; Aharonson, O., Gerstell, M.F., Tatsumi, L., 2007. Three decades of slope
704 streak activity on Mars, *Icarus*, 191, 132-140.

705

706 Smith, D., Neumann, G., Ford, P., Arvidson, R.E., Guinness, E.A., Slavney, S., 1999. Mars
707 Global Surveyor Laser Altimeter Precision Experiment Data Record, NASA Planetary Data
708 System, MGS-M-MOLA-3-PEDR-L1A-V1.0.

709

710 Szathmáry, E., Horváth, A., Sik, A., Bérczi, Sz., Ganti, T., Pócs, T., Kereszturi, A., 2005.
711 Signs of water runoff and its relation to possible living organisms on Mars, 5th EANA
712 Workshop on Astrobiology, Budapest.

713

714 Szathmary, E., Ganti, T., Pocs, T., Horvath A., Kereszturi, A., Berzci, Sz., Sik, A. 2007. Life
715 in the dark dune spots of Mars: a testable hypothesis, in *Planetary Systems and the Origin of*
716 *Life*, ed. Ralph Pudritz, Paul Higgs, Jonathan Stone, Cambridge University Press.

717

718 Titus, T.N., 2005. Thermal infrared and visual observations of a water ice lag in the Mars
719 southern summer, *Geophysical Research Letters*, 32, Issue 24, CiteID L24204. DOI:
720 10.1029/2005GL024211.

721

722 Titus, T., 2008. Infrared observations of mars south polar water ice. Mars Water cycle
723 Workshop, Paris.

724

725 Wagstaff, K.L., Titus, N.T., Ivanov, A.B., Castano, R., Bandfield, J.L., 2008. Observation of
726 the north water ice annulus on Mars using THEMIS and TES, Planetary and Space Science,
727 56. 256-265.

728

729 Wettlaufer, J.D., M.G. Worster, 2006. Premelting Dynamics, Annual Reviews, 38, 427-452.

730

731 Figure captions

732

733 Fig. 1. Comparison of MOC (top) and HiRISE (middle, bottom) images of the same terrains
734 at different dates, showing the similar phenomenon was observed by MGS and MRO. Top
735 row shows 300x300 m insets of MGS MOC image R07-00938 ($L_s = 220^\circ$), middle row shows
736 300x300 m insets of HiRISE images PSP-003609-1110 ($L_s = 232^\circ$) of the same terrains. In the
737 bottom row 80x80 m segments are visible in magnified version of the middle row, which
738 locations are indicated by black boxes. North is up, the Sun illuminates from the left

739

740 Fig. 2. Example for characteristic morphology of slope streaks. Left: distinction between fan-
741 shaped (gray) and confined (black) slope streaks based on their appearance and direction of
742 elongation on an 125x125 meter part of HiRISE image no. PSP_003175_1080. Right:
743 examples for branching morphology of streaks and accumulated pond-like termination. The
744 images are visible up and the graphical representations at bottom

745

746 Fig. 3. Development of two passive streaks (top and bottom rows) on 300x300 m sections of
747 HiRISE images no. 3432-1115, 3643-1115, 3709-1115 (from left toward right), acquired at
748 $L_s = 222.9, 233.2, 236.4$ respectively. Based on the morphology they moved toward the right
749 (toward the elongated part) previously, but currently they show only darkening and the
750 growth of small segments, which finally coalesce into a continuous streak.

751

752 Fig. 4. Change DDSs at three locations in Richardson crater. The 100x100 inset pictures are
753 from HiRISE images (from left to right image no. 3175, 3386, 3597, 3742, 3953, which were
754 acquired at $L_s = 210.6, 220.7, 230.9, 238.1, 248.5$), showing the development of structures.

755

756 Fig. 5. Example images of active streaks from Russel crater. The three images from left to
757 right represent subsequent HiRISE images no. 2482, 2548, 2904 which were acquired at
758 $L_s=178.9$ 181.9 and 197.9 respectively. On the right a graphical representation is visible,
759 showing the movement and its observed speed.

760

761 Fig. 6. Temperature-morphology correlation for Dark Dune Spots and slope streaks in Russel
762 crater, with 300×300 meter sized images of the same terrain are visible at top, where the
763 number of HiRISE images from left to right are 2482-1255, 2548-1255, 2904-1255, which
764 were acquired at $L_s=178.9$, 181.8 , 197.9 respectively. At bottom the temperature curve is
765 indicated (top curve: daytime, bottom curve: nighttime values). Three vertical lines show the
766 temperatures corresponding to the three periods of seasons at the upper images.

767

768 Fig. 7. Temperature-morphology correlation for Dark Dune Spots and slope streaks in an
769 unnamed crater at $68S\ 2E$. Three 100×100 meter insets from HiRISE images are visible up
770 (from left to right image no. 3432, 3643, 3709, which were acquired at $L_s=222.9$, 233.2 ,
771 236.4 respectively) and TES based annual temperature values are visible below.

772

773 Fig. 8. Temperature-morphology correlation for Dark Dune Spots and slope streaks in
774 Richardson crater. Five 100×100 meter insets from HiRISE images are visible up (from left to
775 right image no. 3175, 3386, 3597, 3742, 3953, which were acquired at $L_s=210.6$, 220.7 ,
776 230.9 , 238.1 , 248.5 respectively) and TES based annual temperature values are visible below,
777 where daytime and nighttime temperatures form two curves on the right.

778

779 Fig. 9. The “Sandwich model” of liquid interfacial water (layer thickness d) between ice and
780 surface of a mineral grain.

781

782 Fig. 10. Frost point temperature (thick line) and minimum liquidus temperature (thin curve
783 below) in dependence on the (log of the) number density N of water vapor molecules (water
784 molecules per cubic meter). The small area between the two curves is the “band of
785 undercooled liquid interfacial water” (Möhlmann (2008b) in T- N - phase space).

786

787 Fig. 11. Dependence of the thickness d [m] of the liquid interfacial water layer on the limiting
788 temperature T_l [K] of undercooled water to remain liquid for two Hamaker constant values:
789 $A = 10^{-18}$ J (upper curve) and $A = 10^{-19}$ J (lower curve).

790

791 Fig. 12. Minimum liquid layer temperature for $A = 10^{-19}$ J (upper gray curve) and $A = 10^{-18}$
792 J (lower black curve) in dependence on the layer thickness d . Obviously, liquid interfacial
793 water of about two monolayers in thickness may for appropriate surfaces exist down to about
794 150 K.

795

796 Fig. 13. Li-, Na-, Ca-, and K-Montmorillonites (exp.: thick lines, theor: thin lines), according
797 to experimental data of Anderson (1968) and by using eq. (5). Fig. 13. Li-, Na-, Ca-, and K-
798 Montmorillonites (exp.: thick lines, theor: thin lines), according to experimental data of
799 Anderson (1968) and by using eq. (5). a) Li-montmorillonite reaches up to about 0.8 g/g
800 (uppermost curve), b) Na-montmorillonite reaches up to about 0.65 g/g (lower right curve), c)
801 Ca-montmorillonite reaches up to about 0.55 g/g, and d) K-montmorillonite (very similar to
802 Ca-montmorillonite, b) reaches up to about 0.4 g/g (nearly overlapping curves in the middle).

803

804 Fig. 14 Geometric slope insulation situation.

805

806 Fig. 15. Maximum diurnal downslope flow distance L [m] in dependence on slope inclination.
807 ($R = 10^{-5}$ m, $rP = 3000$ kg m⁻³, $rW = 1000$ kg m⁻³).

808

Table 1.

crater	image no.	date	Ls
Russel (54S 12E)			
	2482_1255	2007.02.05 15:52	178.9
	2548_1255	2007.02.10 16:00	181.8
	2904_1255	2007.03.10 15:57	197.9
unnamed crater (68S 2E)			
	3432_1115	2007.04.20 15:55	222.9
	3643_1115	2007.05.07 15:51	233.2
	3709_1115	2007.05.12 15:56	236.4
Richardson (72S 180E)			
	3175_1080	2007.03.31 16:08	210.6
	3386_1080	2007.04.17 16:04	220.7
	3597_1080	2007.05.03 16:00	230.9
	3742_1080	2007.05.15 15:49	238.1
	3953_1080	2007.05.31. 15:42	248.5

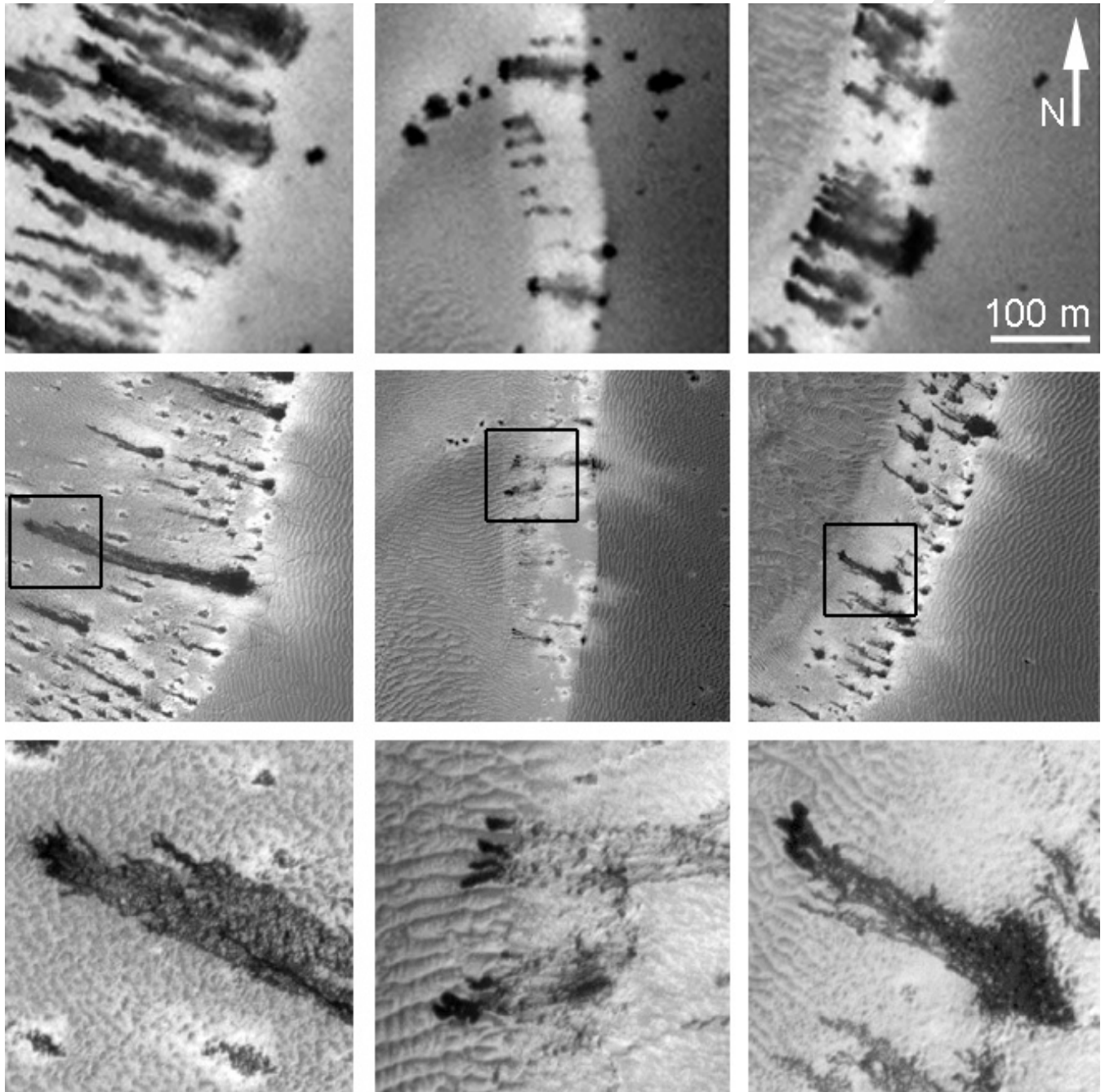


Fig01

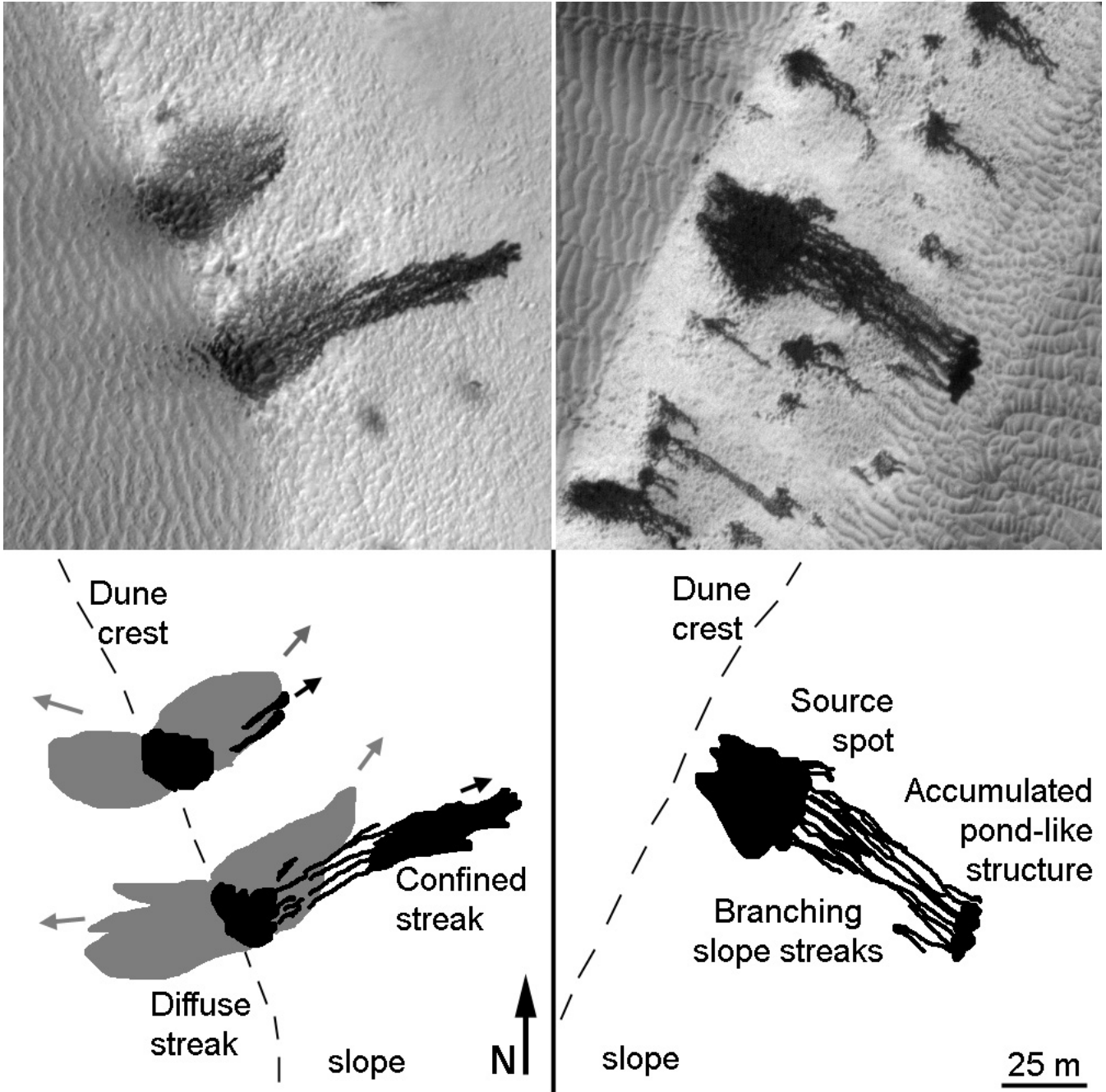


Fig02

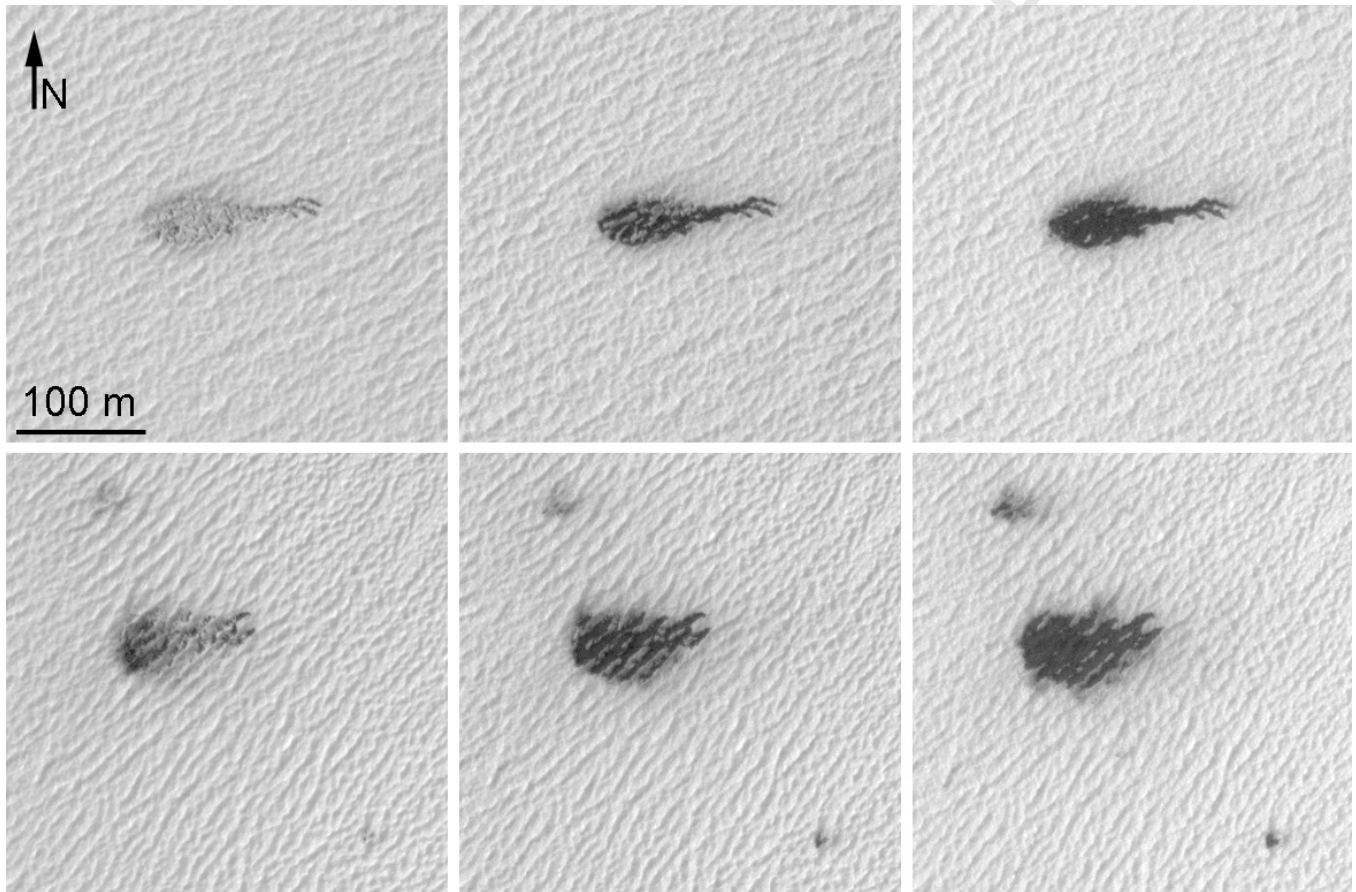


Fig03

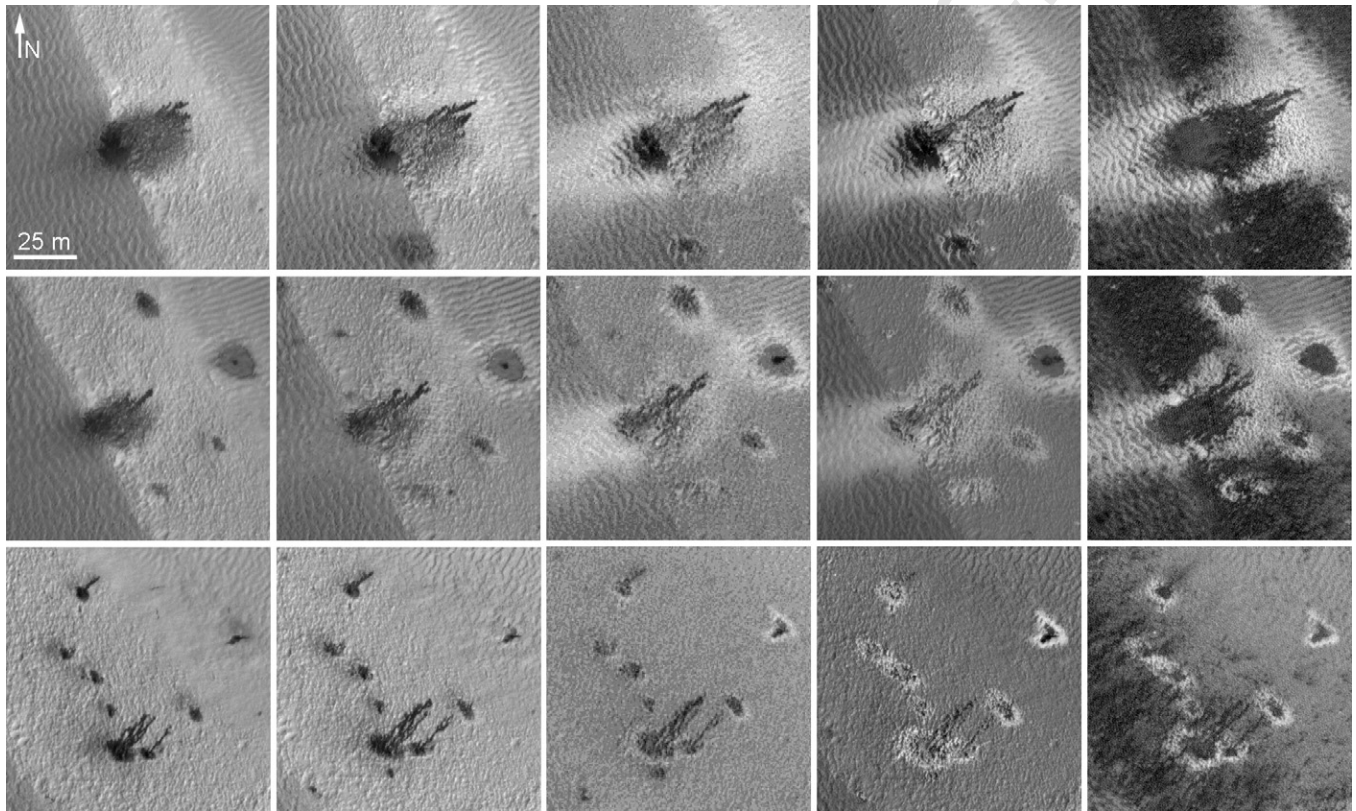


Fig04

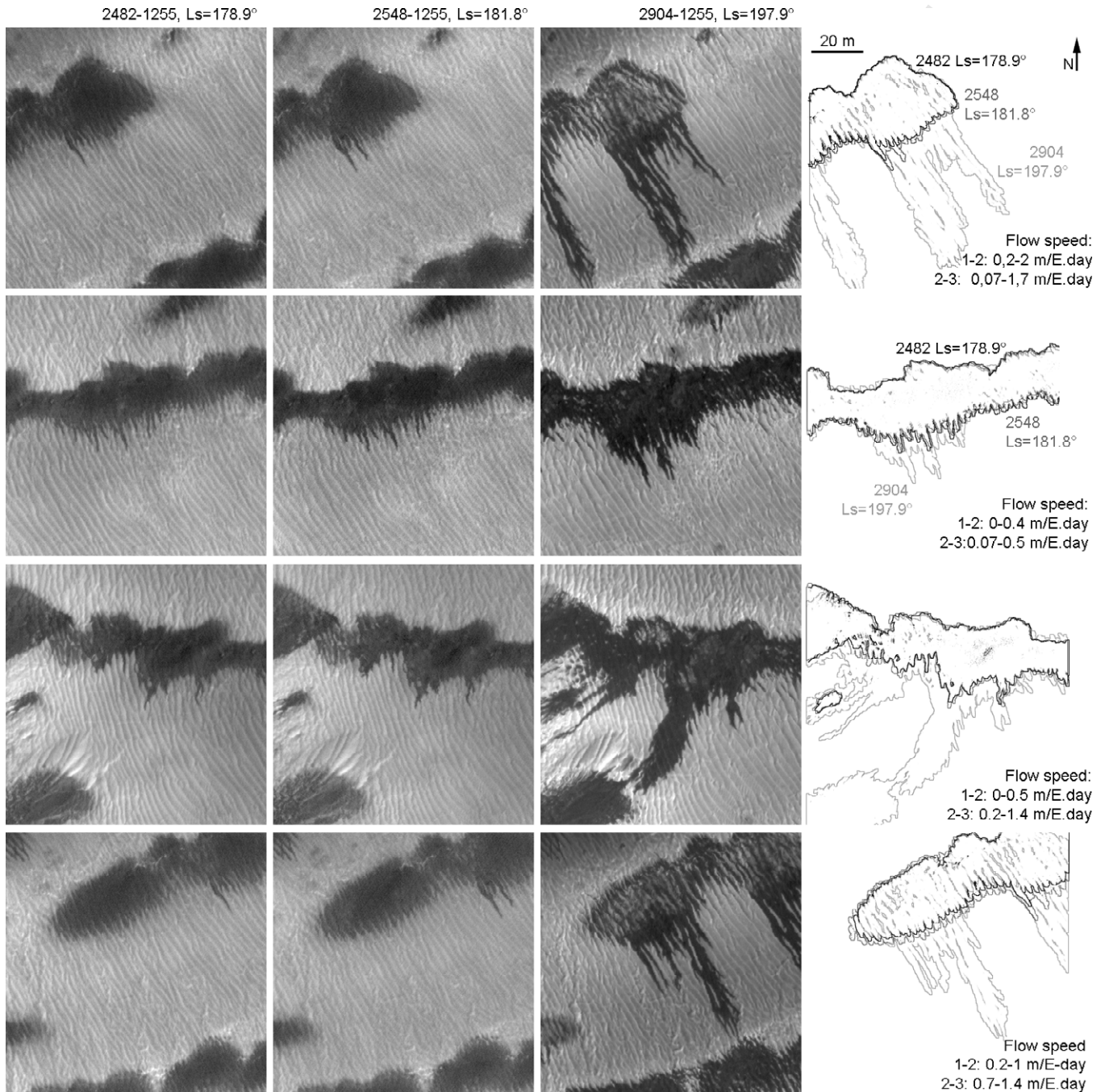


Fig05

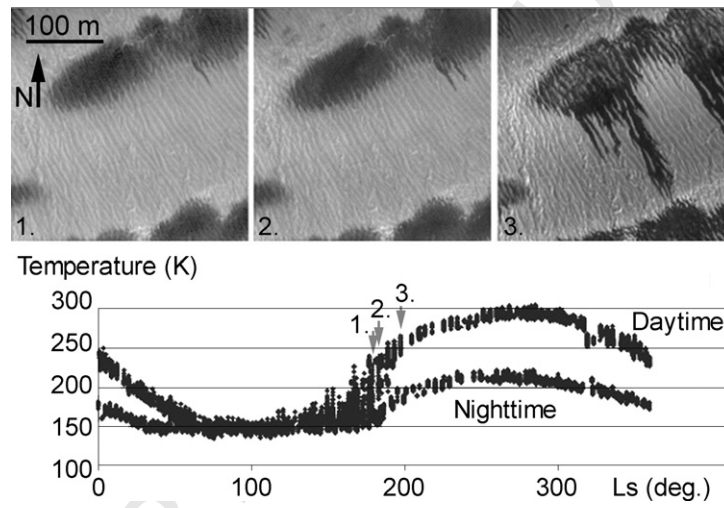


Fig06

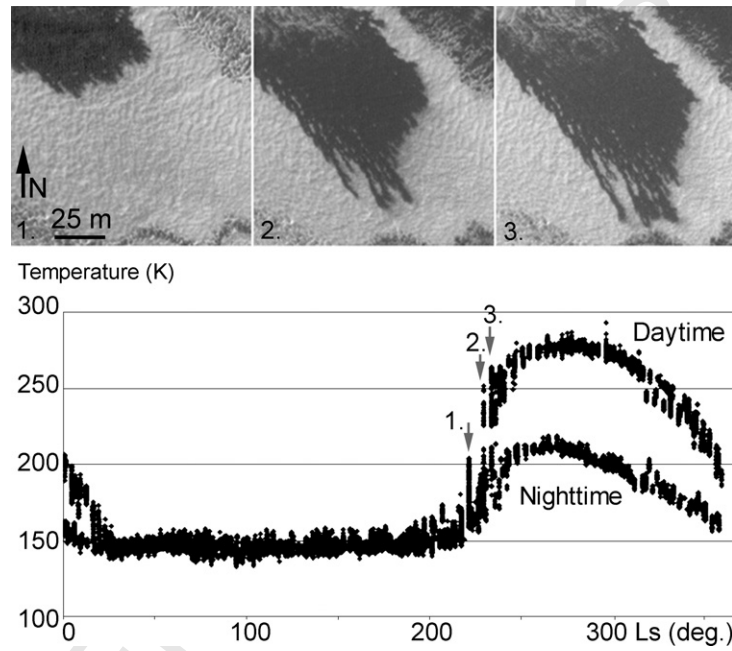


Fig07

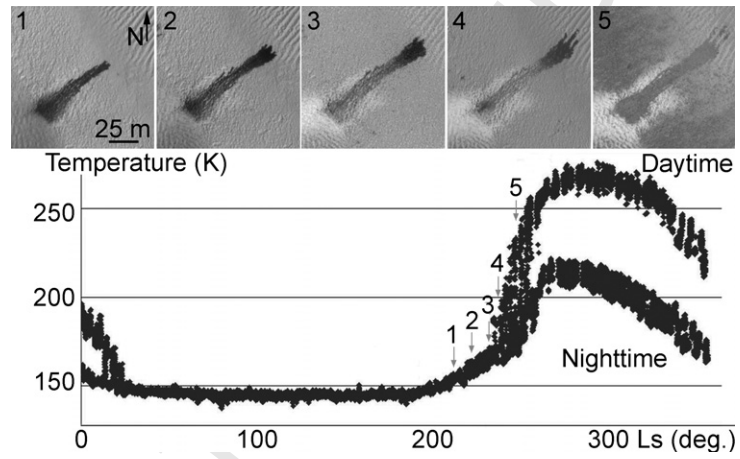


Fig08

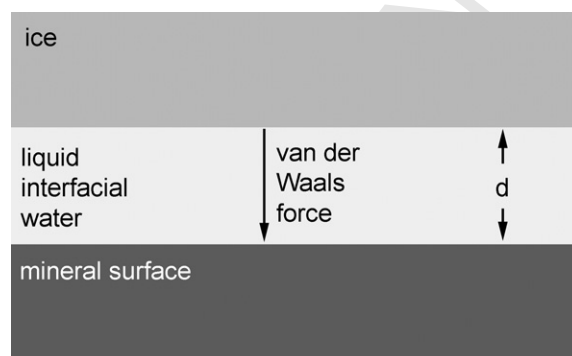


Fig09

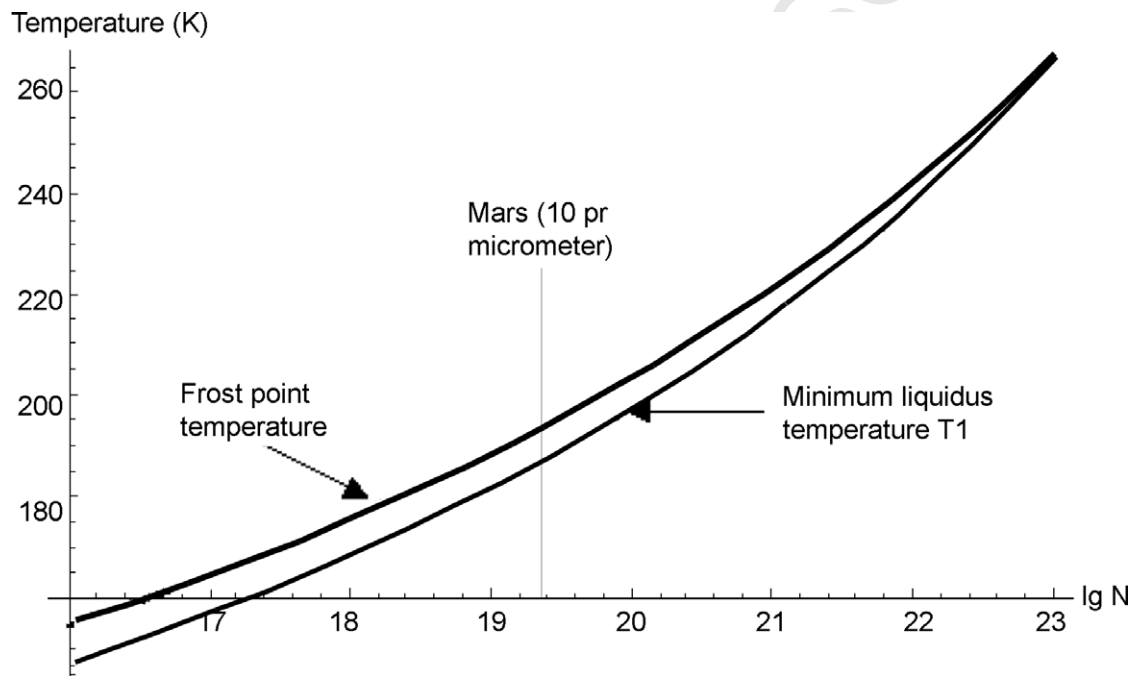


Fig10

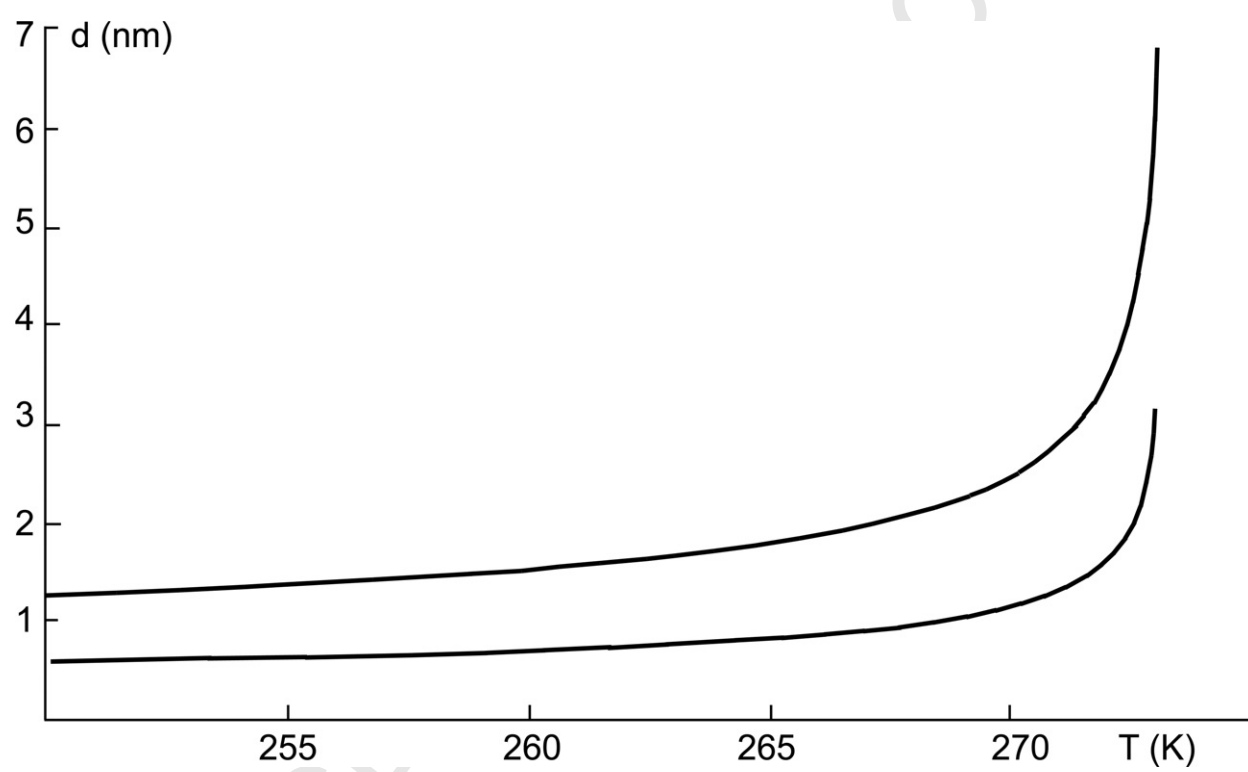


Fig11

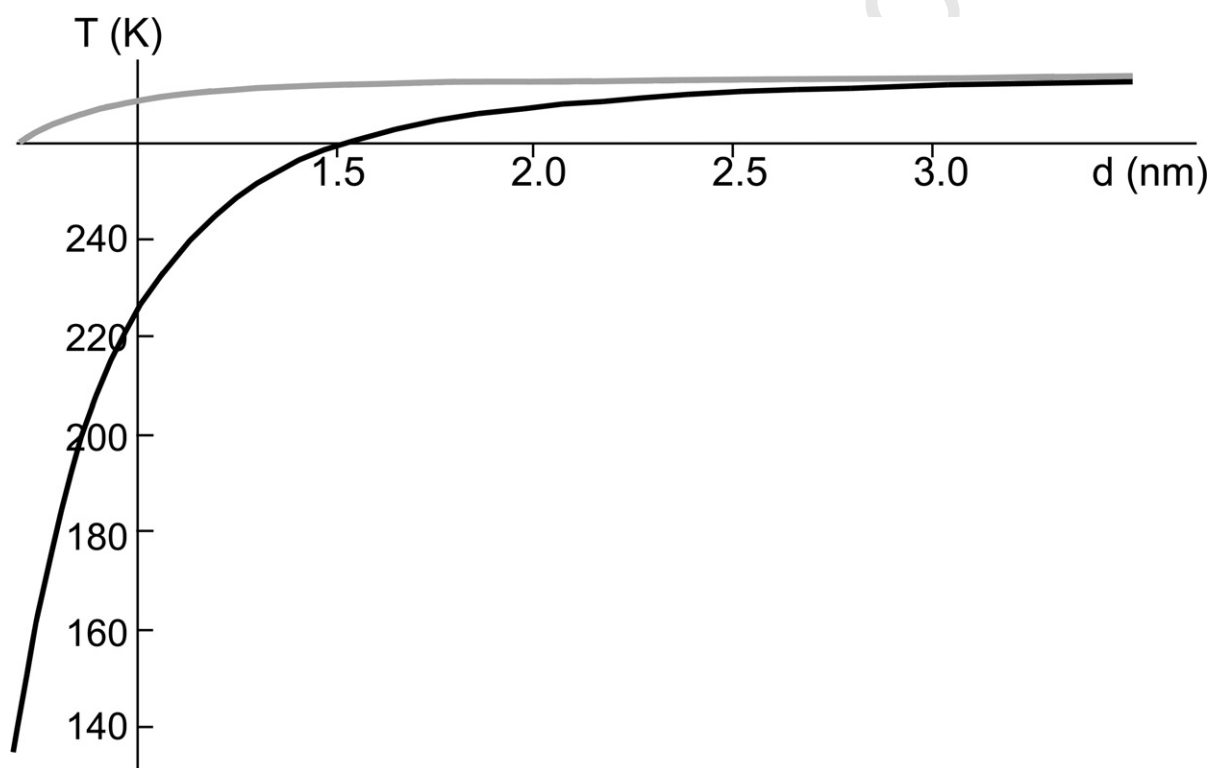


Fig12

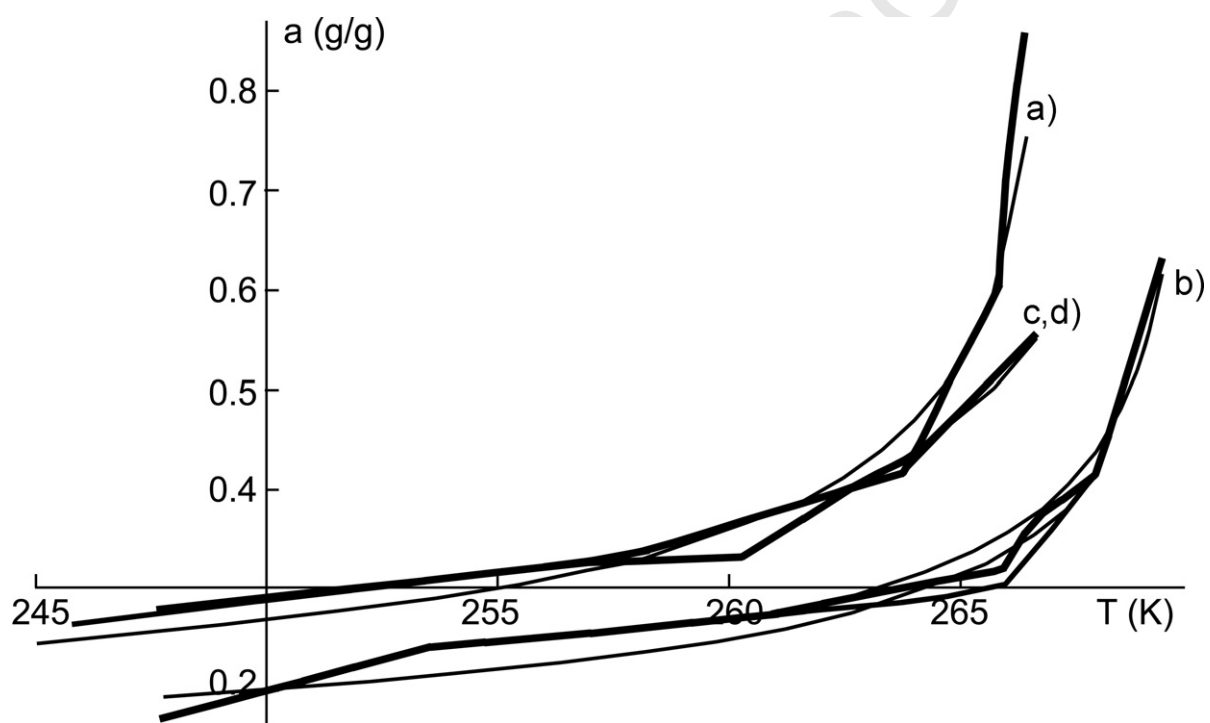


Fig13

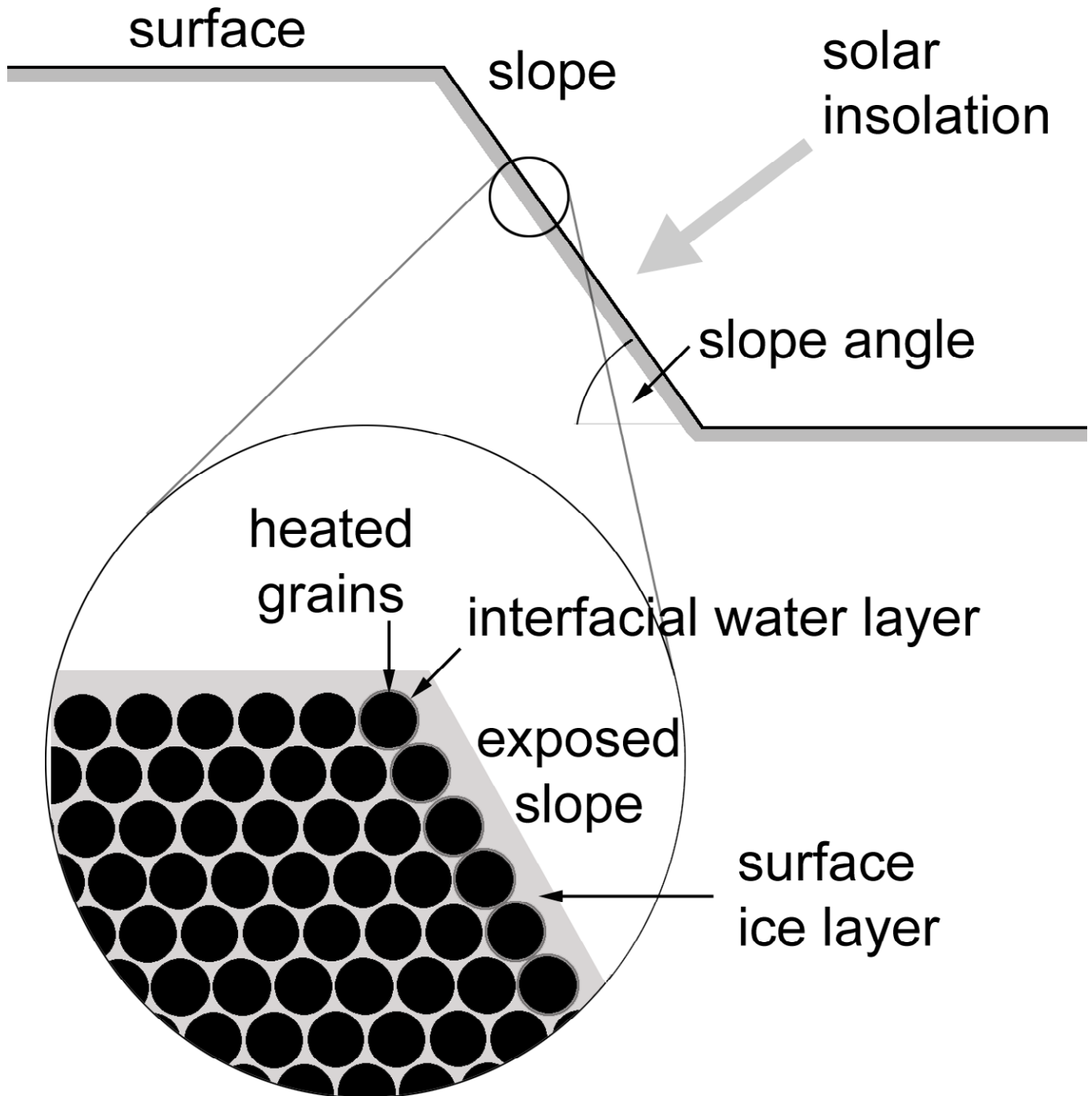


Fig14

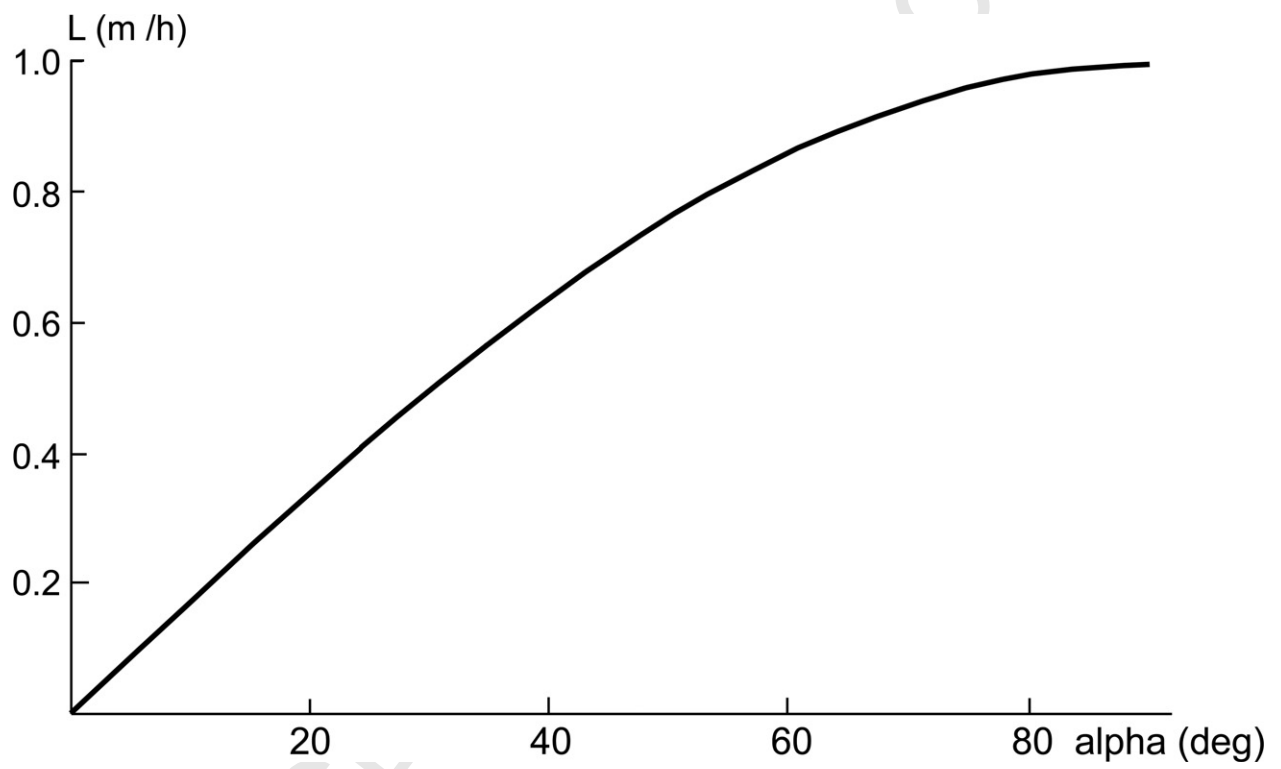


Fig15